ISABE-2005-1304

# PULSE DETONATION ENGINE IMPULSE AND DETONATION SENSITIVITY ANALYSIS FOR PARTIALLY OXIDIZED JET FUEL

F. Pintgen and J.E. Shepherd
Graduate Aeronautical Laboratories
California Institute of Technology
Pasadena, CA 91125 USA

## Abstract

We investigate the ideal single-cycle, single-tube pulse detonation performance of partially oxidized jet fuel. The analysis is based on a sequence of ideal combustion and mixing processes using thermodynamic computations based on a realistic set of product species and thermochemical properties. The calculated specific impulse of partially-oxidized fuel is compared to the reference case of detonating the original fuel in air. Partially oxidized fuel always has a smaller impulse than the original fuel and the specific impulse increases with increasing partial oxidation equivalence ratio. For a partial oxidation equivalence ratio of 2, the impulse is reduced to about 60% of the reference case; for a partial oxidation equivalence ratio of 4, the impulse is reduced to 80% of the reference case.

In the second part of the present study, we report numerical simulations, analysis, and experimental studies of detonation cell width of the mixtures investigated in the first part. We find that the detonation cell width is predicted to be a minimum for a partial oxidation equivalence ratio $\Phi_b$ of approximately 3. This minimum is shown to be a consequence of thermodynamic and chemical kinetic factors, mainly that the largest mole fractions of $H_2$ and CO occur after the primary burn for $\Phi_b \sim 3$. Detonation cell size measurements with synthetic mixtures of partial oxidation products and air were carried out in the Caltech 280-mm diameter detonation tube for partial oxidation equivalence ratios of 2 and 3. This data and numerical computations are used to estimate minimum detonation cell widths of 22-24 mm at 1 atm and 3-9 mm at 6 atm, depending on the initial temperature (24-404°C). Comparison with estimated cell widths for the detonation of a representative hydrocarbon fuel (propane) without partial oxidation indicate that, at best, a factor of two reduction in detonation cell size can be achieved by partial oxidation.

## Introduction

A requirement of commercial aviation applications of pulse detonation engines (PDE) is the use of the standard aviation kerosene or jet fuel. One of the key challenges is the initiation of detonation in mixtures of jet fuel and air. The C4-C12 hydrocarbon mixtures that make up jet fuel have been difficult to detonate reliably in laboratory experiments using low energy techniques based on flame acceleration or modest initiator tube sizes. One approach to solving this problem is by modifying the fuel properties through partial oxidation. This will produce CO, $H_2$, and small hydrocarbon molecules that may be easier to detonate [1] than the original hydrocarbons making up the jet fuel, but also result in a reduced impulse. The aim of the present study is to quantify these competing effects.

We use ideal models of combustion and mixing to compute the single-cycle performance of an ideal PDE using partially oxidized fuel. A total of 81 cases are examined with rich partial oxidation equivalence ratios of 2, 3, and 4 and overall equivalence ratios of 0.8, 1, and 1.2. Initial conditions are pressures between 1-6 atm and temperatures between 25-400°C.

We take as the basis for evaluating detonability the magnitude of the detonation cell width. We describe a combined experimental and numerical approach to estimating the detonation cell size $\lambda$ for a mixture of partially oxidized aviation kerosene and air. The estimation is based on extrapolating a limited number of detonation tube experiments with synthetic partial oxidation products (mixtures of hydrogen-carbon monoxide-nitrogen) and air, discussed in the Cell Size Measurement section. A correlation is developed between the numerical reaction zone length $\Delta$ and experimental cell width $\lambda$. A detailed reaction mechanism and realistic thermochemistry are used with a one-dimensional ZND model to predict reaction zone lengths for the experimental conditions and conditions appropriate to the actual PDE application.

## Model Process

The fuel is modeled as a single notional species $C_{12}H_{24}$ which has a molar mass of 168.3 g/mol and a H/C ratio of 2, similar to the average composition of generic jet fuel. The enthalpy and entropy variations as a function of temperature, which are necessary inputs for the equilibrium solver, were derived by approximating the specific heat capacity at constant pressure by the standard tabulated values for Jet-A [2]. The effective heat of formation (-438.7 kcal/mol) was derived by solving the enthalpy balance equation for the stoichiometric reaction

$$C_{12}H_{24} + 18(O_2 + 3.76N_2) \rightarrow 12CO_2 + 12H_2O + 67.68N_2$$

at standard conditions and using an assumed heat of combustion equal to 42.8 MJ/kg. The thermodynamic computations were carried out using STANJAN [3] and a set of 40 product species. A sequence of ideal processes is used to model the pre-oxidation and detonation process, Fig. 1.

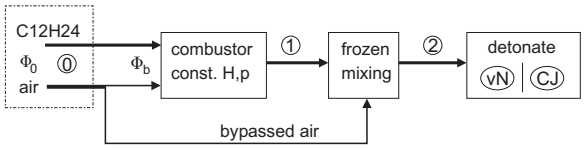


Fig. 1: Schematic of process flow considered. The designation of the various states is given by the circled numbers. The detonation state is divided up in the post-shock (von Neumann state) and the CJ state.

We consider a range of initial pressures $P_0$ = 1, 3, 6 atm and initial temperatures of $T_0$ = 24, 204, 404°C. The sequence of processes is: A) fuel is preburned in air at constant pressure and enthalpy under rich conditions to produce state 1. B) the resulting products are mixed (frozen product composition) with air at constant pressure and enthalpy to achieve a near-stoichiometric mixture at state 2. C) The mixture of partial-oxidation products and air is detonated at Chapman-Jouguet (CJ) conditions to yield the CJ state. The post-shock (von Neumann) conditions are denoted with the subscript *vN*. Three different stoichiometry ratios $\Phi_0$= 0.8, 1, 1.2 of the incoming fuel-air mixture are considered. This corresponds to an overall mixture of composition at state 0 of

$$\Phi_0\, C_{12}H_{24} + 18(O_2 + 3.76N_2).$$

Bypassed air, Fig. 1, leads to a rich mixture at the combustor inlet. Stoichiometry ratios $\Phi_b$=2, 3, 4 are analyzed, leading to a mixture at state 1 of

$$C_{12}H_{24} + (18/\Phi_b)(O_2 + 3.76N_2).$$

The precombustion process for $\Phi_b$=3 and $\Phi_0$=1 can be approximately written as

$$C_{12}H_{24} + 6(O_2 + 3.76N_2) \rightarrow 12CO + 12H_2 + 22.56N_2,$$

and the detonation process as

$$\underbrace{12CO + 12H_2 + 22.6N_2}_{\text{primary burn hot products}} + \underbrace{12O_2 + 45.1N_2}_{\text{bypassed air}} \longrightarrow \underbrace{12H_2O + 9CO_2 + 3CO + 2O_2 + 67.7N_2}_{\text{detonation products}}.$$

In this example, we have used approximate compositions and only major species. In our actual computations, a complete set of species was used for the numerical computations of chemical equilibrium states in order to specify the composition.

The properties of the expansion wave are calculated using a similarity solution leading to the pressure $P_4$ at the thrust wall as discussed in [4]. The pressure differential at the thrust surface and the model prediction

$$I = 4.3\frac{\Delta P}{U_{cj}}V \qquad (1)$$

leads to the impulse per unit volume $I_V=I/V$ where $\Delta P=P_4-P_0$ [1]. The expansion process between the detonation and the end wall was assumed to occur with a shifting equilibrium state so that the species were in equilibrium at all points on the isentrope. Due to this shift in the composition and the dependence of the heat capacity on temperature, the usual perfect gas (constant specific heat ratio) formulas may not be applicable in these cases. To examine this issue, we carried out the isentropic expansion calculations by numerically evaluating the integral

$$u_3 = \int_{p_{cj}}^{p_4} \frac{1}{\rho c}\, dp \qquad (2)$$

to find $P_4$. The velocity $u_3=U_{cj}-c_3$ is the flow velocity just behind the detonation wave, and $c_3$ is the sound speed behind the detonation wave. A linear regression analysis of the isentrope showed that for

[1] Note that the state labels in [4] are slightly different than those used in the present study. In particular, the state at the end of the Taylor wave was labeled state 3 in [4].

all the cases calculated, the results of this exact analysis differed from the perfect gas analysis by at most 1%.

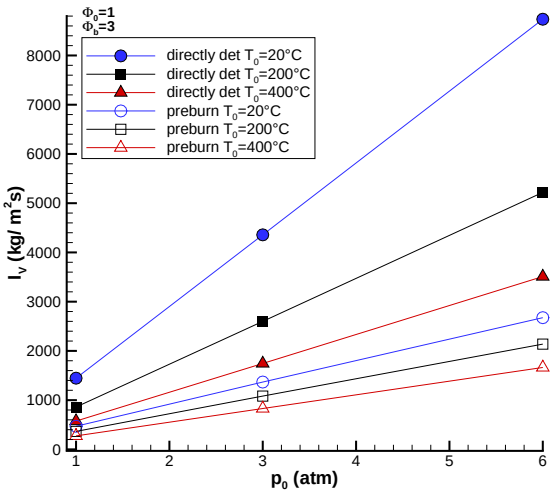


a)

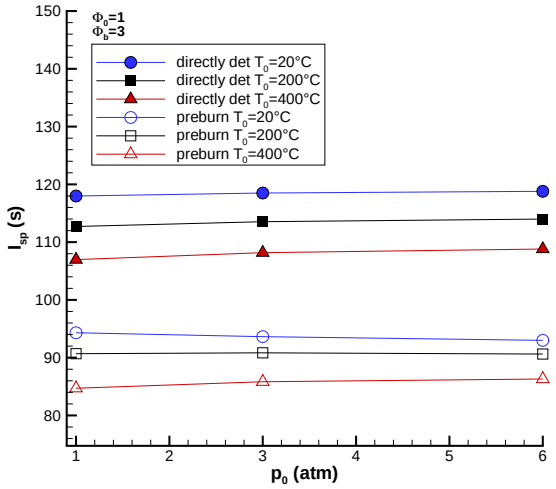


b)

Fig. 2: Impulse per unit volume (a) and mixture specific impulse (b) variation with initial pressure for preburning with $\Phi_0$=1 and $\Phi_b$=3. The reference case for $\Phi_0$=1 is also shown.

## Impulse Calculations

A total of 81 cases are considered. In addition to the variation in overall and preburn equivalence ratio, initial temperatures $T_0$ of 293, 473, and 673 K and initial pressures of $P_0$ of 1, 3, and 6 atm were examined. For reference, we computed the specific impulse obtained by omitting the partial-oxidation step and simply detonating the initial overall mixture at state 0 with $\Phi_0$. For these cases, $\Phi_b$ is irrelevant but, in the plots, these data points are located at $\Phi_b$=3 for comparison.

The variation of impulse with initial pressure is shown in Fig. 2 for the reference and preburn case and the case of $\Phi_0$ = 1 and $\Phi_b$=3. The most significant observation is that the impulse for the partially oxidized fuel is significantly lower than that of the original fuel. The amount of reduction is found to be a stronger function of the preburn equivalence ratio $\Phi_b$. In the cases shown in Fig. 2, the specific impulse of the partially oxidized fuel ($\Phi_b$=3) is about 80% of the original fuel. This reduction is discussed in more detail below and is due to both the lower chemical energy content of the partially oxidized fuel in comparison to the parent molecule and also the higher temperature (thermal energy) of state 2 in comparison to the initial state 0.

The initial pressure and temperature trends shown in Fig. 2 are similar to those for ordinary fuels in air and are discussed in detail by [4]. The impulse per unit volume $I_V$ increases linearly with initial pressure at fixed initial temperature and the impulse per unit mixture mass $I_{sp}$ is essentially independent of initial pressure. The specific impulses are defined as

$$I_{sp} = \frac{I}{V \rho_2 g} = \frac{I_V}{\rho_2 g} = \frac{I}{M g} \qquad (3)$$

where $M$ is the total mass of the combustible mixture to be detonated at state 2 and $g$ is the standard earth gravitational acceleration. In addition to the mixture specific impulse, the fuel specific impulse $I_{spf}$ is also often used in performance analyses

$$I_{spf} = \frac{I}{M_f g}, \qquad (4)$$

where $M_f$ is the initial mass of fuel at state 0. The fuel specific impulse and the mixture-based specific impulse vary only slightly with initial pressure for fixed $\Phi_0$ and $\Phi_b$, see [19] and the discussion in [4].

All impulse measures, $I_V$, $I_{sp}$, and $I_{spf}$, are increasing with increasing preburn stoichiometric ratio $\Phi_b$ as shown in Fig. 3. This is due to the higher energy content of the mixtures at state 2 with a richer preburn mixture. There are two components to this effect. First, as the amount of oxygen in the preburn process decreases, the product composition shifts from $H_2O$ and $CO_2$ to $H_2$ and CO and unburned hydrocarbons [19], which have a higher energy content (enthalpy of formation). Second, the temperature of the mixture state 2 is decreasing with increasing stoichiometry ratio $\Phi_b$. The lower temperature and the higher specific energy content lead to an increase in the specific impulse $I_V$ with increasing $\Phi_b$. This dependence can be justified by examining how the specific impulse depends on the energy content of the mixture that is detonating.

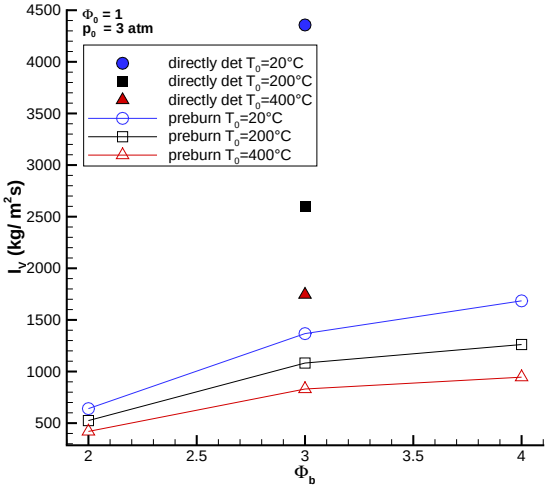


a)

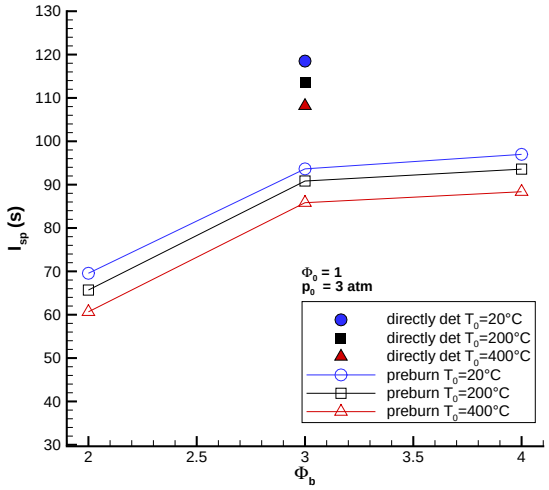


b)

Fig. 3: Impulse per unit volume (a) and mixture specific impulse (b) variation with stoichiometry $\Phi_b$ of the preburn process. Initial pressure of 3atm and overall equivalence ratio of $\Phi_0$=1.

Under the conditions that the CJ pressure is large compared to the ambient pressure, it can be shown [4] by using the one-$\gamma$ model that the impulse scales as

$$I \propto M\sqrt{q_2} \qquad \text{or} \qquad I_{sp} \propto \sqrt{q_2}\,, \qquad (5)$$

where $M$ is the initial mass of the combustible mixture in the detonation tube and $q_2$ is the effective energy release[2] per unit mass of mixture. The major product distributions of state 2 were used to compute the specific heat of combustion $q_c$ and the specific energy release $q_2$ for the mixture of the products of partial oxidation and air. The specific energy release $q_2$ of the mixture to be detonated can be written as [4]:

$$q_2 = \frac{\gamma R T_2}{2(\gamma^2-1)}\left(M_{cj} - \frac{1}{M_{cj}}\right). \qquad (6)$$

Since, in the reference case, the mixture at state 0 is detonated, the index 2 in Eq. 6 is identical to index 0 for the reference case. As shown in Table 1, the effective heat of combustion $q_c$ and the effective energy release $q_2$ do indeed increase with increasing $\Phi_b$, explaining the qualitative trend.

Quantitatively, these considerations also correctly predict that the impulse is essentially identical for mixtures with $\Phi_b$ = 3 and 4, which have similar values of $q_2$ and $q_c$ as shown in Table 1. However, the impulse decreases more rapidly with decreasing $\Phi_b$ than the considerations about $q_2$ alone predict, and the reduction in impulse between pure fuel and partial-oxidation products is larger than expected on this basis.

| $\phi_b$ | $q_c$ | $q_2$ | $I_{sp}$ | $I_{sp}/I_{sp,ref}$ | $\sqrt{q_c/q_{c,ref}}$ | $\sqrt{q_2/q_{2,ref}}$ |
|---|---|---|---|---|---|---|
| 2 | 1.81 | 2.20 | 70 | 0.587 | 0.814 | 0.753 |
| 3 | 2.39 | 3.03 | 94 | 0.789 | 0.936 | 0.884 |
| 4 | 2.43 | 3.33 | 97 | 0.818 | 0.944 | 0.927 |
| Ref | 2.72 | 3.88 | 119 | 1 | 1 | 1 |

Table 1: Calculated heat of combustion $q_c$ [MJ/kg] and specific energy release $q_2$ [MJ/kg] (per unit mass of fuel-air mixture) considering only major species ($N_2$, $O_2$, $C_{12}H_{12}$, $H_2$, CO, $CO_2$, $H_2O$, $CH_4$), for different $\Phi_b$ and fixed $\Phi_0$=1, $T_0$=297K. Reduction in $I_{sp}$(s) compared to reference case ($I_{sp}/I_{sp,ref}$) is only predicted qualitatively by the impulse scaling based on Eq. 5.

The discrepancy between the predicted scaling of the impulse with the energy content (Eq. 5) can be accounted for by reconsidering the dependence of the impulse on detonation properties. For large Mach numbers $M_{cj}$, the detonation velocity can be approximately calculated as

$$U_{cj} \approx \sqrt{2(\gamma^2-1)q}\,, \qquad (7)$$

the detonation pressure is

[2] Due to dissociation, specific heat dependence on temperature, and the difference in average molar mass of reactants and products, the specific energy release is, in general, not equal to the ideal energy release based on the heat of combustion. For complete combustion of stoichiometric $C_{12}H_{24}$-air, the heat of combustion is 2.72 MJ/kg

$$P_3 = P_2 \frac{\gamma M_{cj}^2 + 1}{\gamma + 1}, \qquad (8)$$

where the detonation Mach number is $M_{cj} = U_{cj}/c_2$ and the sound speed ahead of the detonation is c_2 = $\sqrt{\gamma R T_2}$ . The pressure at the end of the Taylor wave is approximately

$$P_4 \approx P_3 \left( \frac{2\gamma}{\gamma + 1} \right)^{-\frac{2\gamma}{\gamma - 1}}. \qquad (9)$$

In terms of these quantities, the specific impulse can be written

$$I_{sp} \propto \frac{c_2}{M_{cj}} \left( \frac{P_4}{P_3} \frac{P_3}{P_2} - 1 \right). \qquad (10)$$

For values of $\Phi_b$ less than 3, the detonation Mach number decreases substantially as $\Phi_b$ decreases due to both the increase in $T_2$ and $q_2$. The resulting variation in $P_3/P_2$ with detonation Mach number causes the specific impulse to fall rapidly as $\Phi_b$ is decreased below 2.

To obtain a quantitative measure of this effect, we need to proceed more carefully than in the original scaling analysis of [4] (pp.32-33). The pressure at the end of the Taylor wave is exactly

$$P_4 = P_3 \left[ 1 - \left( \frac{\gamma - 1}{\gamma + 1} \right) \left( 1 - \frac{U_{CJ}}{c_4} \right) \right]^{-\frac{2\gamma}{\gamma - 1}}. \qquad (11)$$

The specific impulse model of Eq. 1 can then be expressed as

$$I_{sp} = \frac{K}{g} \left[ \frac{1}{\gamma + 1} U_{cj} \frac{P_4}{P_3} - \frac{R T_2}{U_{cj}} \left( \frac{1}{\gamma + 1} \frac{P_4}{P_3} - 1 \right) \right], \qquad (12)$$

where $R$ is the specific gas constant at state 2, and $K$ is a parameter which has a weak dependence on the properties of the mixture, $K(g,q/RT_2)$, here taken as 4.3 [4]. For large Mach numbers $M_{cj}$ and low temperatures $T_2$, the second term can be neglected and the scaling results of [4](pp.~32-33) are recovered. However, in the present situation, the detonation Mach numbers are rather modest and since the temperature upstream of the detonation is much higher than usual, the second term plays an important role.

This can be verified by examining the numerical values for the terms in the impulse equation, Eq. 12.

Considering a mixture with $\Phi_0$=1, $P_0$=3 atm, and $T_0$=293K, the calculated detonation velocity for the preburned case ($\Phi_b$=3) is lower and the pressure ratio $P_4/P_3$ is higher than for the corresponding reference case, Table 2. The dominant parameter, which is responsible for the reduction in impulse for the preburned case, is $R\,T_2$ in the second term of Eq. 12. That can be seen by evaluating Eq. 12 with the quantities given in Table 2:

$$\text{preburned case}: I_{sp}[s] = 139.7 - 46.8 = 92.9,$$

$$\text{reference case}: I_{sp}[s] = 134.5 - 16.3 = 118.2$$

Due to the simplifications used in calculating $R$ in Table 2, the specific impulse $I_{sp}$ calculated using Eq.12 differs slightly from the more precise $I_{sp}$ calculated using Eq. 1, which is given in Table 2 and the appendix. The molecular weight of the major species at state 2 in the preburned case, CO and $H_2$, is lower than in the reference case, $C_{12}H_{24}$ and $O_2$, leading to a higher specific gas constant for the preburned case. Due to the significantly higher temperature $T_2$ of the mixture to be detonated and the higher specific gas constant in the preburned case, the predicted specific impulse is reduced to 79% of the reference case value.

| | preburned | reference |
|---|---|---|
| $T_2$ (K) | 651.48 | 297.00 |
| $R$ (J/kgK) | 340 | 273 |
| $U_{cj}$ (m/s) | 1678.1 | 1797.6 |
| $M_{sj}$ | 3.35 | 5.52 |
| $c_4$(m/s) | 915.70 | 928.80 |
| $P_4/P_3$(Eq.11 | 0.418 | 0.377 |
| $I_{sp}$ (s) (Eq.1) | 93.8 | 118.6 |

Table 2: Calculated parameters for the preburned ($\Phi_b$=3) and reference case and specific impulse. $\Phi_0$=1, $T_0$=297K. The gas constant $R$ is calculated based on the reactant molar mass

For fixed composition and initial pressure, the impulse varies inversely with initial temperature

$$I \propto \frac{V}{T_2}. \qquad (13)$$

Due to the decrease in the mixture temperature $T_2$ with increasing initial temperature$T_0$, the impulse per unit volume decreases with increasing initial temperatures $T_0$ (see Fig. 4). The mixture-specific impulse $I_{sp}$ is decreasing less in comparison than the $I_V$ with increasing initial temperature, $T_0$, since only the dissociation of the products contributes to the slight decrease in specific impulse. The impulse per unit volume decreases slightly with increasing stoichiometric ratio $\Phi_0$ in the region considered $\Phi_0$ =0.8-1.2 (Fig. 4). This is due to the higher temperature of the mixture at state 2 and the relation given in Eq. 13. The mixture-specific impulse reaches its maximum for $\Phi_0$=1 for the cases considered.

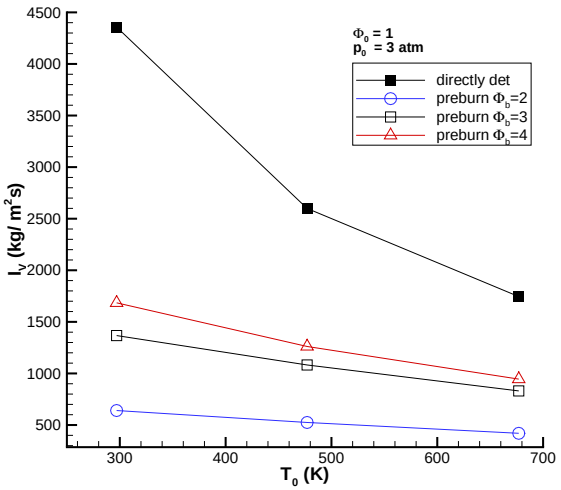


a)

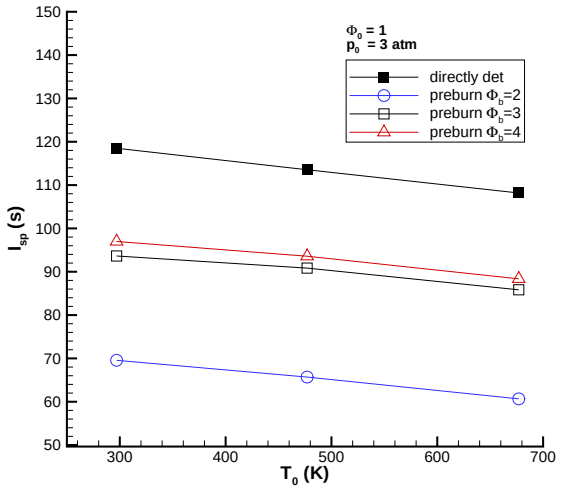


b)

Fig. 4: Impulse per unit volume (a) and mixture specific impulse (b) variation with initial temperature $T_0$. $P_0$ = 3atm and $\Phi_0$ = 1.

## Comparison with Partial Oxidation of JP10

The results of the present study are closely related to previous experimental work on JP10 ($C_{10}H_{16}$) partial oxidation by [5]. In that study, a two-stage constant-volume combustion process was carried out in a fashion analogous to that described in Fig. 1. First, partial oxidation was carried out in a constant-volume explosion step for equivalence ratios between 2.5 and 4.5. Second, following cooling of the reaction products, air was added to bring the overall stoichiometric ratio to one. Third, a second constant-volume explosion was carried out. The peak pressure reached during the second explosion step was used to define a figure of merit for chemical energy release from partially oxidized mixtures. Note that the peak pressure in the constant-volume explosion is very similar in value to the pressure at the end of the Taylor wave which is used to determine impulse in the ideal single-cycle model.

The "effectiveness" of the partial-oxidation step can be defined [5] as the ratio of the peak pressure in the second explosion to the peak pressure of the explosion of the reference case of a stoichiometric JP10-air mixture. The effectiveness varied from 60% to 94% as the equivalence ratio of the partial-oxidation step was varied from 2.5 to 4.5. This is similar to the variation in relative impulse with $\Phi_b$ that is presented in Table 1.

The measured peak pressure in the second explosion was about 10% less than computed equilibrium peak pressures. Those results indicate that the thermochemical prediction methods of the present report will give reasonable estimates of single-cycle efficiency for a range of initial equivalence ratios $\Phi_b$ that are larger than some minimum value of about 2.5. The upper limit on $\Phi_b$ is not known and will depend on the design of the burner used for the partial-oxidation step.

## Induction Zone Length Calculations

The induction zone length is defined as the distance between the leading shock wave and the point of the most rapid temperature increase. Unless otherwise specified, the shock is considered to be propagating at the CJ velocity. The reaction zone structure was calculated with the one-dimensional ZND model [6] using the standard gas-phase chemical kinetics library of [7]. The 37-species reaction mechanism of [8] was used to describe the chemical reaction rates. The thermodynamic conditions and composition for the primary burn and the subsequent mixing with air were obtained from the thermodynamic equilibrium calculations [3].

A complete set of plots of the induction zone length and cell size as a function of $\Phi_0$, $\Phi_b$, $T_0$, and $P_0$ is given in [9]. The induction zone length varies with initial conditions and composition in a complex fashion. In general, the induction zone length decreases with increasing initial pressure but can either increase or decrease with increasing initial temperature. The dependence on the composition variable $\Phi_b$ is not monotonic and a minimum reaction zone length occurs at intermediate values, see [9] for more detail.

## Induction Zone Length Dependence on $\Phi_b$

In order to investigate the influence of the preburn equivalence ratio $\Phi_b$ on the induction zone length $\Delta$, a series of calculations for $1.5<\Phi_b<4.5$ in increments of

0.05 was conducted. As shown in Figs. 5 and 6, there is a minimum in Δ near $\Phi_b$~3 for nearly all $\Phi_0$, $T_0$ and $P_0$ considered in this study. The minimum Δ = 0.49 mm is found at $\Phi_b$ = 3.05 for $\Phi_0$ = 1, $T_0$= 24°C, $P_0$=1bar. At 3 and 6 atm (see Figs. 5 and 6), Δ is weakly dependent on composition in the interval $2<\Phi_b<4$. At 1 atm, the minimum is quite pronounced and the location is independent of initial temperature.

The dependence of Δ on $\Phi_b$ and the existence of a minimum is due to the variation of the species and thermodynamic properties of state 2, the mixture of combustion products, and bypass air, see Fig. 1. The major species are shown as a function of $\Phi_b$ in Fig. 7 for $T_0$=24°C and $P_0$=1 atm.

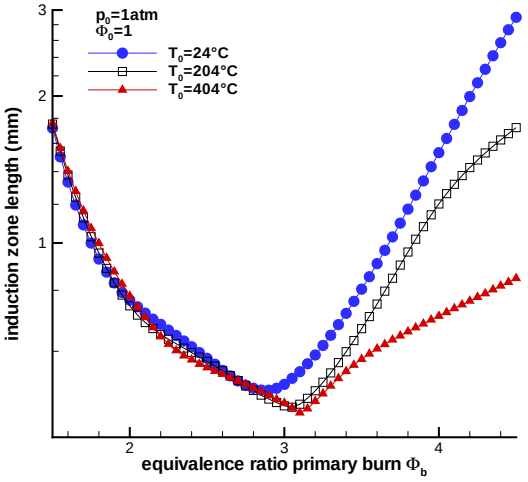


Fig. 5: Induction zone length Δ as a function of $\Phi_b$ for $\Phi_0$ = 1, 3, and 6 atm at $T_0$=204°C.

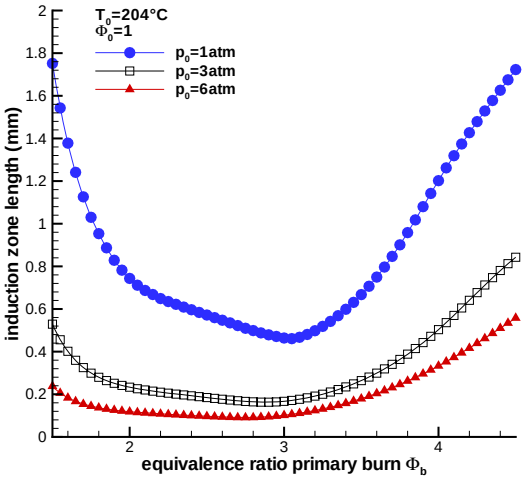


Fig. 6: Induction zone length Δ as a function of $\Phi_b$ for $\Phi_0$ = 1, $P_0$= 1 atm, and $T_0$= 24, 204, and 404°C.

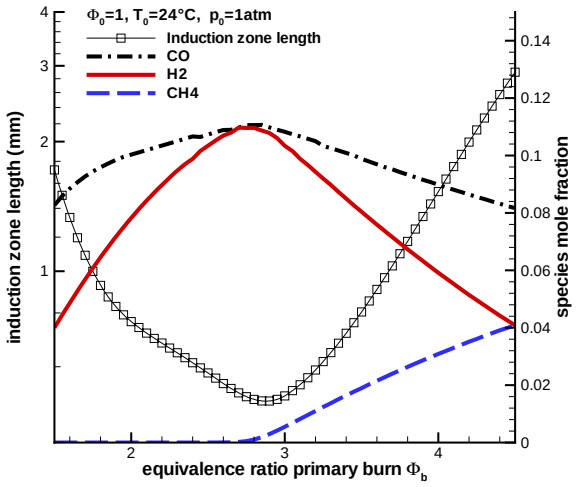


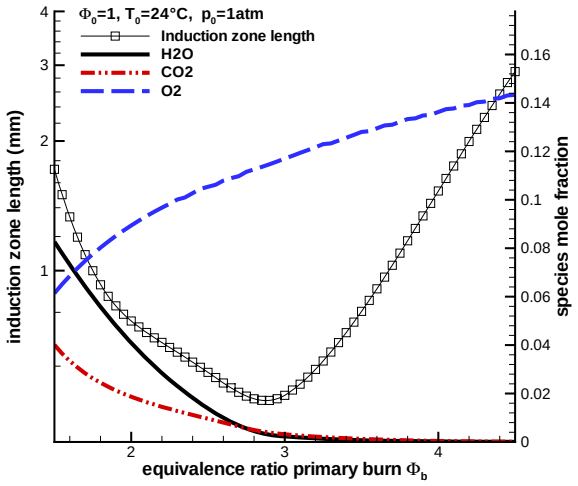


Fig. 7: Mole fractions of major species (except $N_2$) at state 2 as a function of $\Phi_b$ for $\Phi_0$=1, $T_0$= 24°C, $P_0$=1 atm. The induction zone length is shown for reference.

The key to understanding the $\Phi_b$ dependence of the reaction zone length is to recognize the shift in reactant composition in state 2 with $\Phi_b$, Fig. 7. For values of $\Phi_b<3$, the reactants are limited in the amount of both CO and $H_2$ and oxidizer ($O_2$) as $\Phi_b$ decreases to 1. For values of $\Phi_b>3$, the amount of $H_2$ and CO decreases with increasing $\Phi_b$ and the composition is dominated by the higher hydrocarbons. The density and temperature of the *vN* state decrease with increasing $\Phi_b$ between 1 and 3. For values of $\Phi_b>3$, the temperature and density are essentially independent of $\Phi_b$.

Altogether, we see that as we increase $\Phi_b$ from 1, the reaction zone length at first dramatically decreases since fuel and oxidizer are present in increasing amounts until $\Phi_b$ = 3 is reached. This

accounts for the rapid drop in reaction time and Δ with increasing $\Phi_b<3$ since the change in composition dominates over the decreasing temperature and density, which, for fixed composition, would tend to increase the reaction time. With further increases in $\Phi_b>3$, there is insufficient oxygen so that the amount of CO decreases and the excess C atoms combine with $H_2$ to form higher hydrocarbons, in the present case $CH_4$. The reaction time for $CH_4$ is much longer than for the CO-$H_2$ mixtures and an increasing function of the concentration of hydrocarbon fuel [1]. The *vN* density and pressure are essentially constant for $\Phi_b>3$ so that the increase in reaction zone length with $\Phi_b$ is due entirely to the shift in composition from CO-$H_2$ to a mixture dominated by higher hydrocarbons.

The quantitative results shown are increasingly questionable with increasing equivalence ratio since the reaction mechanism is not intended to treat this range of compositions. Only a limited number of higher hydrocarbons were included in the computation and it is known that soot formation (not modeled) is an important process for $\Phi_b>2$. However, we expect that the results are qualitatively correct and that a minimum in the reaction zone length should exist near $\Phi_b=3$. This is just a consequence of the oxygen balance in the reactants and should not depend on the details of the product composition.

Empirical Model of Induction Time

In order to explain these trends, we appeal to a simple empirical model of the induction zone length. The model is based on the notion of an induction time $t_i$ that is associated with the chemical reaction processes behind the shock front. The induction zone length Δ corresponds to the distance the fluid particle is convected during the induction time, $\Delta = w_{vN}\, t_i$. If we assume that the fluid has a constant post-shock velocity $w_{vN}$ in the shock fixed reference frame and the induction time $t_i$ can be modeled with an Arrhenius-type dependence

$$t_i = A\rho_{vN}{}^{\alpha} \exp\frac{E}{RT_{vN}}, \qquad \Delta = Aw_{vN}\,\rho_{vN}{}^{\alpha} \exp\frac{E}{RT_{vN}}, \tag{14}$$

where $A$ is a scaling constant, $\rho_{vN}$ and $T_{vN}$ are the von Neumann density and temperature, $\alpha$ is an exponent (negative) modeling the density effect on collision rate, $R$ is the gas constant, and $E$ is the activation energy.

Determining the Parameters

The constants $A$, $\alpha$, and $E$ depend on the combustion regime and specific mixture composition. Computations using the CJ-ZND model with realistic thermochemisty and detailed reaction mechanism are used to determine $T_{vN}$, $\rho_{vN}$, $w_{vN}$, and Δ. A perturbation procedure with the ZND model, described below, is then used to obtain $\alpha$ and $E$. Equation 14 is then evaluated to find the constant $A$.

The activation energy $E$ and the density exponent $\alpha$ are calculated by evaluating numerically the induction time for a perturbation in $T_{vN}$ and $\rho_{vN}$ assuming the Arrhenius-type dependence given in Eq. 14:

$$\frac{E}{R} = \frac{\ln t_{ia} - \ln t_{ib}}{1/T_a - 1/T_b}, \quad \alpha = \frac{\ln t_{ia} - \ln t_{ib}}{\ln \rho_a - \ln \rho_b}, \tag{15}$$

where $t_{ia}$ and $t_{ib}$ are induction times corresponding to the perturbed temperatures $T_a$ and $T_b$ as well as the perturbed densities $\rho_a$ and $\rho_b$, so $T_{a/b}=T_{vN} \pm 0.01T_{vN}$. Temperature and pressure perturbations were considered independently. This leads to a more accurate activation energy than the method [10] of perturbing the shock Mach number, since the post-shock density is not constant with varying shock velocity. The perturbation magnitude has to be large enough to avoid the influence of numerical errors and small enough to reflect a good approximation at the given thermodynamic condition. A perturbation of smaller than 0.1% and larger than 10% on $T_{vN}$ and $\rho_{vN}$ found to give erratic results.

The Minimum in Δ Revisited

Using this model, the existence of a minimum in Δ can be explained qualitatively by considering the parameters of the induction zone length model, Eq. 14. The two competing terms primarily influencing Δ as a function of $\Phi_b$ are $\rho_{vN}{}^{\alpha}$ and $exp(E/R\ T_{vN})$, which have opposite trends when varying $\Phi_b$, Fig. 8.

The term $\rho_{vN}{}^{\alpha}$ is decreasing for increasing $\Phi_b$ since the negative density exponent decreases in absolute value and $\rho_{vN}$ is increasing, as shown in Fig. 8. The increase in $\rho_{vN}$ is caused by the increase in Mach number, and the increase in $\rho_2$ is due to $T_2$ decreasing with increasing $\Phi_b$. The change in $\alpha$ is mainly caused (Fig. 8) by the change in mixture composition at state 2. It was difficult to obtain numerically a smooth function for $\alpha(\Phi_b)$ with the method described above, despite using the perturbation magnitude of 0.01 obtained from the considerations discussed in Determining The Parameters section. The values for $\alpha$ shown in this section are obtained from a perturbation of 0.05, so the values might not be as accurate when $\alpha$ is changing strongly, as, for example, when $\Phi_b<2$.

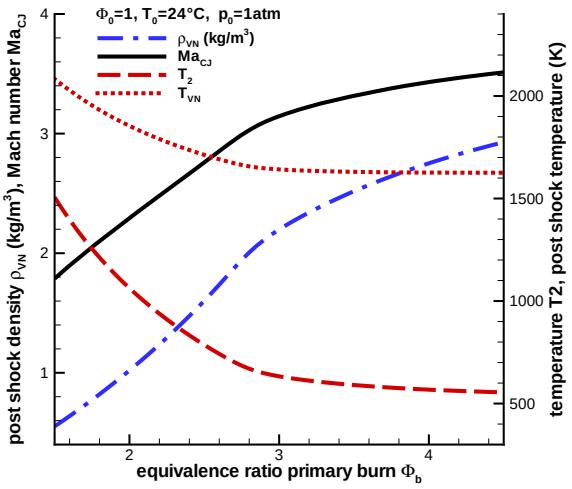


Fig. 8: Shock Mach number, pre-shock temperature $T_2$, post-shock temperature and density variation as a function of $\Phi_b$ for $P_0$=1 atm and $T_0$=24°C .

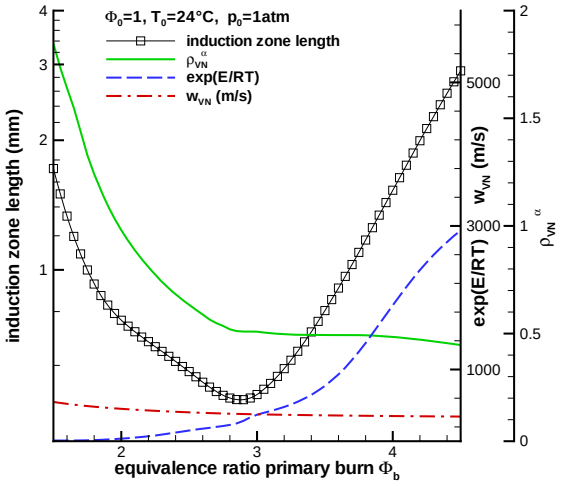


Fig. 9: Terms in induction zone length model evaluated with parameters obtained from simulations. Note that the post-shock velocity in the shock reference frame velocity $w_{vN}$ is almost independent of $\Phi_b$. $T_0$= 24°C, $P_0$= 1 atm, $\Phi_0$= 1.

The factor $exp(E/R\ T_{vN})$ in Eq. 14 is increasing with increasing $\Phi_b$ (Fig. 9) since the activation energy $E$ is a strongly increasing function of $\Phi_b$. The post-shock temperature $T_{vN}$ is approximately constant for $\Phi_b$>3 (Fig. 10), since the increase in Mach number compensates for the decrease in initial temperature.

The term $w_{vN}$ in Eq. 14 does not change significantly (Fig. 9) with $\Phi_b$ in the interval considered. For the interval $\Phi_b$<3, the strongly increasing value of $\rho_{vN}^{\alpha}$ with decreasing $\Phi_b$ is

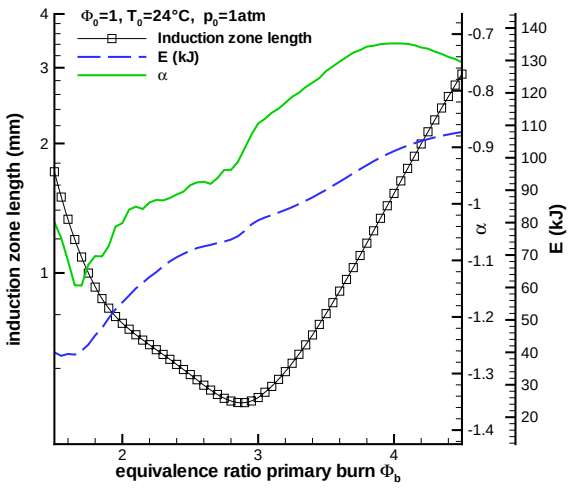


Fig. 10: Activation energy $E$ and density exponent $\alpha$ versus $\Phi_b$. $T_0$= 24°C, $P_0$= 1 atm, $\Phi_0$=1.

dominating the trend of the increasing induction zone length. In the case of $\Phi_b$>3, the strongly increasing values of $exp(E/R\ T_{vN})$ with increasing $\Phi_b$ dictate the dependence of $\Delta$ on $\Phi_b$, since $\rho_{vN}^{\alpha}$ is approximately constant in this region. In the region of the minimum in $\Delta$ for $\Phi_b$~3, both density and Arrhenius terms are slowly varying functions of $\Phi_b$. Note that the minimum is relatively flat for 2<$\Phi_b$<4, and the induction zone length is primarily a function of the initial pressure in this region.

## Induction Zone Length Dependence on $P_0$

The dependence of $\Delta$ on initial pressure and density is shown in Figs. 11 and 12. The calculated induction zone length $\Delta$ decreases by 50-85% (depending on $\Phi_b$ and$T_0$) with the initial pressure $P_0$ increasing from 1 to 6 bar.

In order to illustrate the initial pressure dependence more clearly, the induction zone length was calculated (Fig. 12) for the range $P_0$=1-6 atm in increments of 0.2 for $\Phi_0$ = 1, $\Phi_b$= 4, and $T_0$ = 404°C. The slope in the double logarithmic plot is determined to be -0.70 using a linear regression analysis over the entire pressure interval. Using only the seven data points in the vicinity of $P_0$=1 atm, the slope is determined to be -0.83, which is in good agreement with the density exponent of $\alpha$=-0.853 as determined in a more exact fashion in Determining The Parameters section. The differences can be explained by the neglected $T_{vN}$ dependence on $P_0$ and the fact that $\rho_0$ is not exactly proportional to $\rho_2$ due to changes in the Mach number and inaccuracies in applying the one-gamma model as discussed in [9]. The plot shows the $\Delta$ as a function of the initial density $\rho_0$ and not the density $\rho_2$ just upstream of the detonation.

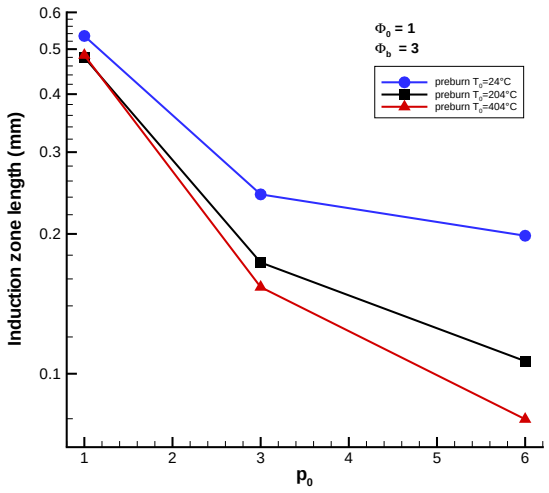


Fig. 11: Calculated induction zone length for $\Phi_0$=1 and $\Phi_b$=3 as a function of $P_0$.

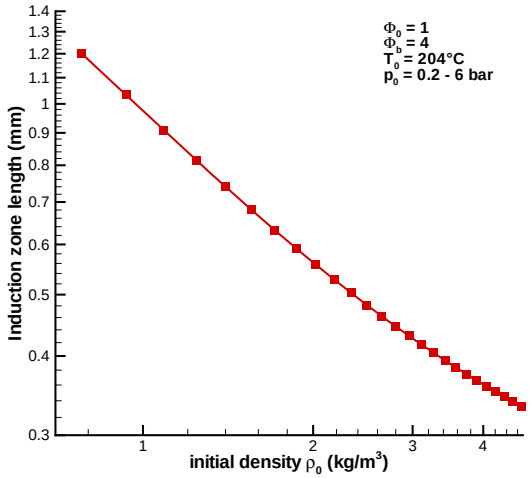


Fig. 12: Dependence of Δ on initial density. The slope in the log-log plot is the density exponent $\alpha$.

Since the composition at state 2 and $w_{vN}$ have only a weak dependence on the initial pressure, the two parameters to be considered in Eq. 14 for the induction zone length dependence on initial pressure are $\rho_{vN}^{\alpha}$ and *exp(E/R* $T_{vN}$*)*. The post-shock density is directly proportional to the initial pressure due to the nearly constant shock Mach number. As a consequence, the term $\rho_{vN}^{\alpha}$ is inversely proportional to the initial pressure. The post-shock temperature $T_{vN}$ is only slightly increasing with increasing initial pressure and, therefore, *exp(E/R* $T_{vN}$*)* is only weakly dependent on the initial pressure in the regimes considered.

## Induction Zone Length Dependence on $T_2$

The induction zone length decreases with increasing initial temperature $T_0$, as shown in Fig. 13. This is due to two effects. First, the temperature $T_2$ increases with increasing $T_0$. Second, the composition of the mixture to be detonated (state 2) varies with temperature since the distribution of species shifts with changing temperature affecting the equilibrium constants. The effects of temperature and composition shift are separately examined in Fig. 14. Each curve represents a fixed composition, determined by the value at the nominal conditions corresponding to the points shown on each curve. As shown, the composition shift is not solely responsible for shorter reaction zones with higher initial temperatures. For higher initial temperatures, the composition shifts from higher hydrocarbons ($CH_4$, $C_2H_4$, etc.) towards $H_2$ and CH [9], leading to a more sensitive mixture. For fixed composition, the reaction zone length decreases with increasing state 2 temperature.

The dependence of detonation cell width and reaction zone length on initial temperature has been examined by [11,12,13], and [14] for hydrogen-air-diluent mixtures. The effect of initial temperature on cell size in $C_2H_2$-$O_2$ mixtures has been studied by [15], $C_2H_4$-$O_2$ mixtures by [16], and $H_2$-$O_2$ mixtures by [17].

The results of these experiments and numerical modeling efforts show that with increasing initial temperature, the reaction zone length and cell size generally can either increase or decrease depending on the composition and, in some cases, the dependence is not monotonic. The results are found to be particularly sensitive to the mixture equivalence ratio and diluent amount with the temperature

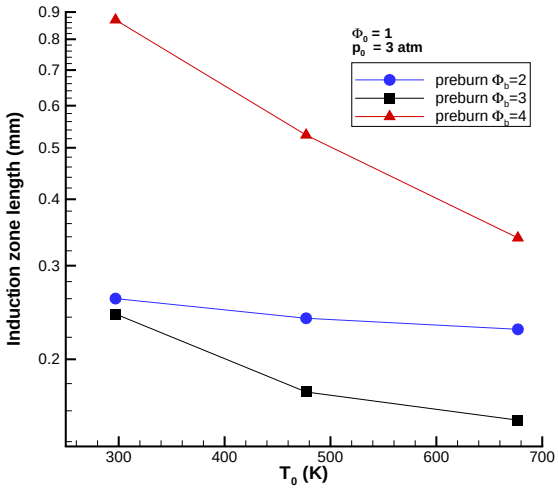


Fig. 13: Calculated induction zone length for $\Phi_0$ = 1, and $P_0$ = 3 atm as a function of $T_0$.

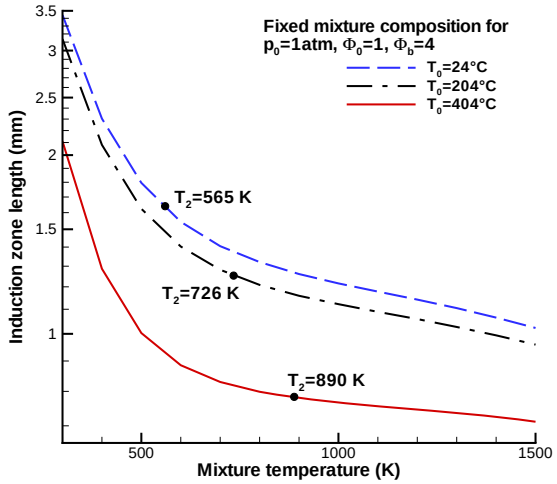


Fig. 14: Induction zone length as a function of temperature $T_2$ for three fixed compositions corresponding to initial temperatures of $T_0$=24, 204, and 404°C. $P_0$=1 atm, $\Phi_0$=1, $\Phi_b$=4.

derivative being positive in some cases and negative in others [13,15]. In the present study, the reaction zone length appears to always decrease with increasing initial temperature but in order to more clearly understand this effect, we have used the simple model of reaction zone length (Eq. 14) to analytically determine the influence of initial temperature variation on density, post-shock temperature, and velocity.

Similar considerations have also been made by [16,15] in the analysis of their data. The present analysis was originally conducted to understand the trends reported by [12]. The analysis is described in detail with an example evaluation in [9]. Using approximations, the dependence of induction zone length on temperature is:

$$\frac{\partial \Delta}{\partial T_2} = \begin{cases} > 0, & \text{for } \dfrac{E}{RT_{vN}} < -\alpha \dfrac{c_{pvN} T_V n}{c_{p2} T_2} \\ < 0, & \text{for } \dfrac{E}{RT_{vN}} > -\alpha \dfrac{c_{pvN} T_V n}{c_{p2} T_2} \end{cases} \qquad (16)$$

## Cell Size Measurement

The cell size measurements were carried out by D. Lieberman of Caltech. The procedure was to detonate mixtures similar in composition to the partial-oxidation products at state 2 in the 280 mm diameter Gaseous Detonation Tube (GDT), see [18], which is 280 mm in diameter and 7.3 m in length. Since our laboratory did not have the capability to actually carry out partial oxidation of Jet A, we explored other methods of synthesizing mixtures with a similar composition to the predicted major species of partial oxidation.

The initial approach for obtaining partial-oxidation products was to burn a fuel-rich mixture of hexane-air in a 400 l vessel. The resulting products are then transferred to the detonation tube, mixed with air to stoichiometric conditions, and detonated. A stronger ignition source than a spark or glow plug is necessary to realize complete combustion of the hexane-air mixture for higher equivalence ratios. A 25 mm diameter, 400 mm long initiator tube equipped with a Shchelkin spiral opens into the side of the 400 l vessel and was filled with stoichiometric propane-oxygen prior to the ignition with a spark plug at the end. The emerging detonation creates a combustion wave in the rich hexane-air mixture. For $\Phi_b$>1.75, even this strong initiator did not lead to complete combustion as observed on the pressure traces. We abandoned this approach and used synthetic mixtures composed of the major products at state 2 (CO, $CO_2$, $H_2$, $O_2$, $N_2$) based on equilibrium calculation predictions. The synthetic mixtures were detonated in the GDT and the cell size was manually measured on soot foils. In total, 10 shots (see Table 3) with varying $N_2$ amounts were performed in order to bracket the cases $\Phi_b$ = 2 and $\Phi_b$ = 3. The cell size measured as a function of the $N_2$ amount $\beta$ are shown in Figs. 12a and b and also Table 3. Cell size measurements were performed for the cases $\Phi_b$=2,3 for $\Phi_b$ = 1. The initial conditions for the synthetic mixtures were 1bar and 295K, so the temperature does not match $T_2$ of the model cycle.

| Shot | $\beta$ | $\lambda$ (mm) | $\delta\lambda_+$ (mm) | $\delta\lambda_-$ (mm) | $U_{cj}$ (m/s) | $\Delta$ (mm) |
|---|---|---|---|---|---|---|
| $\Phi_b = 2$ , $CO + 0.78H_2 + 0.19CO_2 + 0.9O_2 + \beta N_2$ | | | | | | |
| 1764 | 5.0 | 46 | 6 | 13 | 1679 | 0.86 |
| 1765 | 6.0 | 98 | 23 | 23 | 1639 | 1.34 |
| 1760 | 7.0 | 128 | 32 | 15 | 1599 | 2.46 |
| 1763 | 7.5 | 190 | 10 | 20 | 1561 | 4.97 |
| $\Phi_b = 3$ , $CO + H_2 + O_2 + \beta N_2$ | | | | | | |
| 1753 | 4.0 | 14 | 2 | 3 | 1806 | 0.27 |
| 1758 | 5.0 | 26 | 2 | 5 | 1730 | 0.50 |
| 1759 | 5.6 | 30 | 7 | 9 | 1699 | 0.67 |
| 1754 | 6.0 | 33 | 8 | 8 | 1683 | 0.81 |
| 1755 | 7.0 | 59 | 31 | 15 | 1638 | 1.40 |
| 1757 | 7.5 | 97 | 28 | 36 | 1617 | 1.92 |

Table 3: Experimental conditions and results of cell size experiments.

The scaling factor $\lambda/\Delta$ is derived from the induction zone length $\Delta$ calculated for the thermodynamic conditions matching the ones in the experiment,

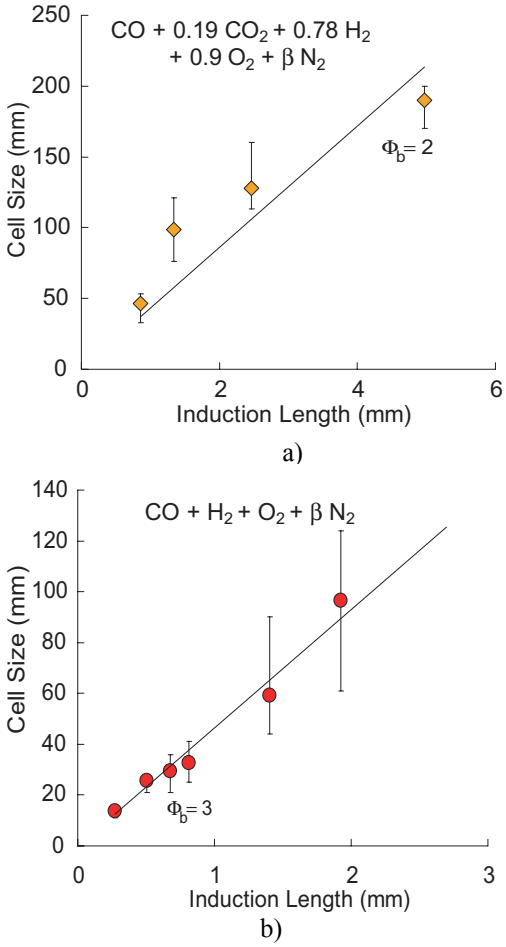


Fig.15: Least-squares linear fit of measured cell size versus calculated induction zone length. a) bracketing the $\Phi_b$=2 case: $\lambda \approx 43\ \Delta$. b) bracketing the $\Phi_b$=3 case: $\lambda \approx 47\ \Delta$.

$T$=295K, $P$=1 atm. For the purpose of estimating the cell sizes for the actual partial-oxidation cases, a constant scaling factor is used for all the cases. The scaling factor $\lambda/\Delta$ was determined by a linear least-squares fit between the measured cell size and the calculated induction zone length for varying $N_2$ amount [9]. For the cases $\Phi_b = 2$ and $\Phi_b = 3$, the scaling factor (Fig. 15) is 42.9 and 46.6, respectively. In the following cell size estimates, a scaling factor of 45 was used for all cases.

## Cell Size Estimation

The cell size $\lambda$ was estimated by multiplying the calculated induction zone length $\Delta$ by the previously determined scaling factor of 45. The dependence of $\lambda$ on the parameters $\Phi_b$, $T_0$, and $P_0$ is, therefore, the same as that of $\Delta$ as discussed in detail previously in the Induction Zone Length Calculations section. A complete set of plots of estimated cell sizes for all conditions and in tabular form is given in [9]. The cell size varies for $\Phi_0 = 1$ and $P_0$=1 atm from $\lambda$=21 mm for $\Phi_b$=3 and $T_0 = 404$°C up to $\lambda$=72 mm for $\Phi_b$=4 and $T_0$=24°C, Fig. 16a. Increasing the initial pressure to 6 atm decreases the cell size, and the estimated range extends from $\lambda$=3mm up to $\lambda$=30 mm, depending on $\Phi_0$, $\Phi_b$, and $T_0$, Fig. 16b.

The minimum in cell size, except for the cases $\Phi_0 = 1$ and $T_0 = 24$°C, always occurs near $\Phi_b = 3$. The value of $\Phi$=3 is close to the value of $\Phi_b$ at which the minimum $\Delta$ is observed. The initial equivalence ratio $\Phi_0$ has a minor influence on the cell size in the interval considered, see Fig. 17. A higher initial temperature tends, in general, to decrease the cell size, so for $\Phi_0 = 1$, $\Phi_b$= 4, and $P_0$=1 atm, the cell size decreases from $\lambda$=72 mm at $T_0$=24°C to $\lambda$=24 mm at $T_0$=404°C. For $\Phi_b$<3, the influence of $T_0$ is less pronounced, see Fig. 18.

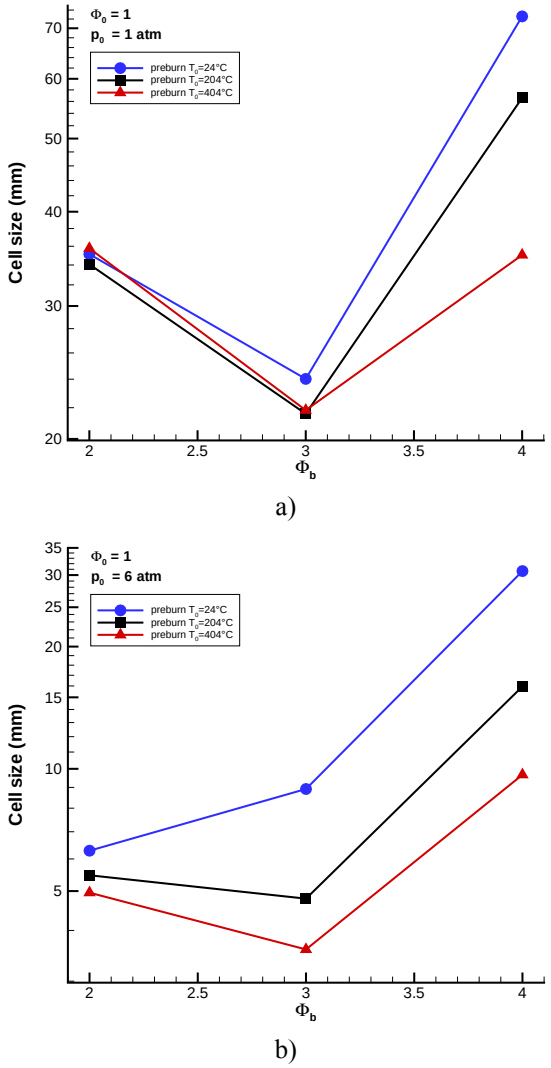


Fig. 16: Estimated cell size for $\Phi_0 = 1$ and a) $P_0$ = 1 atm and b) $P_0$ = 6 atm.

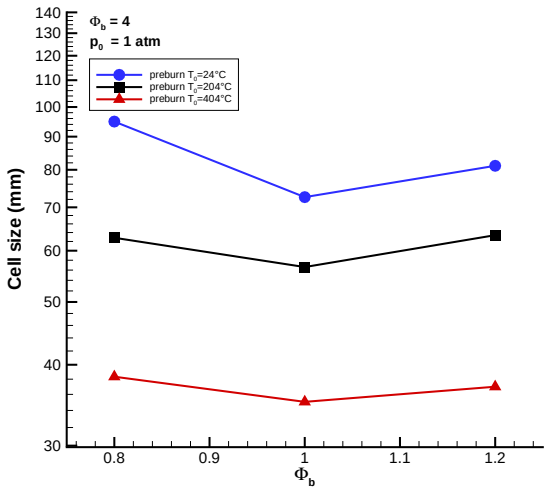


Fig. 17: Estimated cell size as a function of $\Phi_0$.

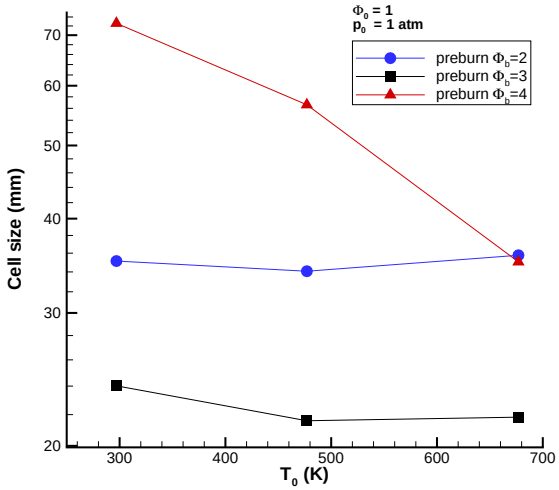


Fig. 18: Estimated cell size as a function of $T_0$ for $\Phi_0$=1 and $P_0$=1atm.

## Summary

The cell size of partially oxidized jet fuel was estimated from an experimentally derived scaling relationship between cell size and calculated induction zone length. The major parameter determining the cell size for the cases considered in this study is the initial pressure of the mixture. The cell size decreases by a factor of up to seven from 22 mm to 3 mm ($\Phi_b$=2, $\Phi_0$=1, $T_0$=404°C) by increasing the initial pressure from 1 to 6 atm. The minimum cell size $\lambda$=3.5 mm is predicted to occur for $\Phi_0$=1, $\Phi_b$= 3, $T_0$=404°C, and $P_0$=6 atm. A higher initial temperature leads, especially for $\Phi_b$>3.5, to lower cell sizes. For a preburn equivalence ratio of $\Phi_b$≈3, the minimum in cell size is observed for practically all cases of $T_0$, $\Phi_0$, and $P_0$ considered. The shallow minimum is in the interval 2<$\Phi_b$<3.5 and the cell size varies up to a factor of two at most. For $\Phi_b$ = 4, the cell size increases up to 35-72 mm, depending on $T_0$ compared to the minimum cell size predicted at $\Phi_b$≈3 of 22-23 mm for $\Phi_0$=1 and $P_0$=1 atm.

The single-cycle pulse detonation performance analysis [19] predicted that the mixture-based specific and fuel specific impulse are essentially identical for $\Phi_b$=3 and 4. By contrast, the predicted cell size increases by a factor of three when changing the preburn equivalence ratio from $\Phi_b$=3 to 4 for all operating conditions considered [9]. An operating regime of $\Phi_b$=3 appears to be the most desirable operational regime. Since the specific impulse is approximately independent of initial pressure and the cell size is strongly decreasing with increasing initial pressure, a high initial pressure yields a sensitive mixture without decreasing the impulse. Choosing the optimum initial temperature is a trade-off between how sensitive the mixture is against how much specific impulse is gained in the cycle. Increasing the initial temperature from 24°C to 404°C decreases the specific impulse up to 15% but can lead to a three times smaller cell size. The decrease in cell size with rising temperature is observed only for $\Phi_b$≈4, which is an undesirable case. In the regime of minimum cell size, $\Phi_b$≈3, the temperature has a negligible influence on the mixture sensitivity [9], and a lower initial temperature is preferable since this yields a higher specific impulse.

## Conclusions

The essential question that we set out to answer with this study was: Will partial oxidation substantially increase detonation sensitivity without significantly decreasing the specific impulse?

### Impulse

This issue was examined at length in the first part of this study [19] and the conclusions reached there are: Partial oxidation of jet fuel reduces the ideal specific impulse relative to the original fuel. Due to the higher temperature of the mixture to be detonated in the preburned case, the volume specific impulse $I_V$ is significantly lowered in comparison to the reference case. The calculated impulses $I_{sp}$ and $I_{spf}$ for the preburn stoichiometry ratio $\Phi_b$=2 are 50-60% of the corresponding impulse calculated for the reference cases, which assume direct initiation without a preburn process. For a highly rich preburn with stoichiometry ratio $\Phi_b$=4, the impulses $I_{sp}$ and $I_{spf}$ reach approximately 78-83% of the corresponding reference case. The calculated impulses, $I_V$, $I_{sp}$, and $I_{spf}$, increase strongly with increasing stoichiometry

ratio $\Phi_b$ of the preburn process up to a value of $\Phi_b$=3. The values for $I_{sp}$ and $I_{spf}$ are essentially identical for $\Phi_b$=3 and 4. Higher initial temperature results in a lower impulse for all of the cases considered.

Detonation Sensitivity

We use computed reaction zone lengths or predicted detonation cell widths to characterize the sensitivity. In order to compare the detonation sensitivity of aviation kerosene-air mixtures with partial-oxidation products and air, we need data on the detonation of aviation kerosene. Very limited data exist on kerosene detonation [20] so, instead, we will use a representative HC fuel, propane, and calculate reaction zone lengths based on the CJ-ZND model and the [21] mechanism. As a check on the detailed reaction modeling, we also used global induction time formulas derived from shock tube experiments by [22]. The results for propane-air have all been converted to predicted cell widths by scaling the 1 atm, 298 K data to the nominal experimental cell width of 55 mm for propane-air. The results are given in Table 4 for the most sensitive partial-oxidation cases, $\Phi_b$=3 and $\Phi_0$=1. The propane-air results are for stoichiometric mixtures.

These results indicate that, at best, a factor of two reduction in the detonation cell width can be achieved by detonating partial-oxidation products mixed with air rather than the original kerosene-fuel mixed with air. There is substantial uncertainty in these results which can only be reduced by shock tube or detonation experiments with kerosene-air mixtures and also partial-oxidation products-air mixtures.

| | | Predicted cell width | | |
|---|---|---|---|---|
| $T_0$ | $P_0$ | Partial Ox. | Konnov | Shock tube |
| (K) | (tam) | (mm) | (mm) | (mm) |
| 297 | 1 | 24.0 | 55.0 | 54.5 |
| 297 | 3 | 10.9 | 19.3 | 25.8 |
| 297 | 6 | 8.9 | 9.9 | 16.3 |
| 477 | 1 | 21.6 | 37.2 | 20.4 |
| 477 | 3 | 7.8 | 14.1 | 9.7 |
| 477 | 6 | 4.8 | 7.6 | 6.2 |
| 677 | 1 | 21.8 | 20.8 | 6.7 |
| 677 | 3 | 6.9 | 8.3 | 3.2 |
| 677 | 6 | 3.6 | 4.7 | 2.1 |

Table 4: Comparison of predicted cell widths for partial-oxidation products of generic jet fuel ($\Phi_b$=3, $\Phi_0$=1) with air and for directly detonating HC fuel, modeled as propane, with air ($\Phi_0$ = 1).

Note that the auto-ignition time of the partially oxidized-air mixture (state 2) is for $\Phi_b$=2, and $T_0$=400°C is in the order of $t_{i,auto}$=50$\mu$s as the mixture is still fairly hot ($T_2$≈1200K). This limits the practical application as it is difficult to mix and fill the thrust tube in this time frame. The auto-ignition time is strongly increasing with decreasing mixture temperature as $t_{i,auto}$≈1ms for $T_2$=950K. The calculated constant pressure combustor temperature is an upper bound and the actual temperature of the mixture at state 2 will be lower than the ideal calculated value. For all other cases $\Phi_b$≥3, the temperature $T_2$ was calculated to be significantly lower (down to 520K) and the auto-ignition time is no limitation for the practical application.

## References

Thank you to Daniel Lieberman for the contributions regarding the cell size measurements. This work was carried out for General Electric under contract GE-PO A02 81655 under DABT-63-0-0001.

## Bibliography

[1] J.M. Austin and J.E. Shepherd. *Detonations in hydrocarbon fuel blends.* Combust. Flame, 132, 73-90, 2003.

[2] Anon, *Aviation Fuel Properties, CRC580*, ASME, 1983.

[3] W.C. Reynolds. *The element potential method for chemical equilibrium analysis: Implementation in the interactive program STANJAN, version 3.* Technical report, Dept. of Mechanical Engineering, Stanford University, Stanford, CA, January 1986.

[4] E. Wintenberger, J. M. Austin, M. Cooper, S. I. Jackson and J.E. Shepherd, *An analytical model for the impulse of a single-cycle pulse detonation engine*, Journal of Propulsion and Power, 19(1):22-38, 2003.

[5] M. Cooper and J. E. Shepherd, *Thermal and Catalytic Cracking of JP-10 for Pulse Detonation Engine Applications*, California Institute of Technology, Explosion Dynamics Laboratory Report, FM2002.002, December, 2002.

[6] J.E. Shepherd. *Chemical kinetics of hydrogen-air-diluent detonations.* Prog. Astronaut. Aeronaut., 106, 263-293, 1986.

[7] R. Kee, F. Rupley, and J. Miller. Chemkin II: *A FORTRAN chemical kinetics package for the analysis of gas-phase chemical kinetics.* Technical Report SAND89-8009, Sandia National Laboratory, 1989.

[8] J. Warnatz and V. Karbach. *C2 mechanism for methane-air combustion.* http://www.ca.sandia.gov/tdf/3rdWorkshop/ch4mech.html, 1997.

[9] F. Pintgen and J.E. Shepherd. *Detonation sensitivity of partially-oxidized aviation kerosene.* Explosion Dynamics Laboratory Report FM2003.007, California Institute of Technology, February 2004.

[10] E. Schultz. *Detonation Diffraction Through an Abrupt Area Expansion*. PhD thesis, California Institute of Technology, Pasadena, California, April 2000.

[11] S.R. Tieszen, M.P. Sherman, W.B. Benedick, J.E. Shepherd, R.Knystautas, and J.H. Lee. *Detonation cell size measurements in hydrogen-air-steam mixtures.* In J.R. Bowen, J.-C. Leyer, and R.I. Soloukhin, editors, Dynamics of Explosions, 106:205--219, 1985.

[12] D.W. Stamps, W.B. Benedick, and S.R. Tieszen. *Hydrogen-air-diluent detonation study for nuclear reactor safety analyses.* Technical report, NUREG/CR-5525 SAND89-2398, 1990.

[13] D.W. Stamps and S.R. Tieszen. *The influence of initial pressure and temperature on hydrogen-air-diluent detonations.* Combust. Flame, 83, 353-364, 1991.

[14] G. Ciccarelli, T.G. Ginsberg, and J.L. Boccio. *The influence of initial temperature on the detonability characteristics of hydrogen-air-steam mixtures.* Comb. Sci. and Tech., 128, 181-196, 1997.

[15] Y. Auffret, D. Desbordes, and H.N. Presles. *Detonation structure and detonability of $C_2H_2$-$O_2$ mixtures at elevated initial temperature.* SHOCK WAVES, 11(2), 89-96, 2001.

[16] Y. Auffret, D. Desbordes, and H.N. Presles. *Detonation structure of $C_2H_4$-$O_2$-ar mixtures an elevated initial temperature.* SHOCK WAVES , 9(2), 107-111, 1999.

[17] R. Zitoun, D. Desbordes, C. Guerraud, and B. Deshaies. *Direct initiation of detonation in cryogenic gaseous $H_2$-$O_2$ mixtures.* SHOCK WAVES, 4(6):331-337, 1995.

[18] R. Akbar. *Mach Reflection of Gaseous Detonations*. PhD thesis, Rensselaer Polytechnic Institute, Troy, New York, August 1997.

[19] F. Pintgen and J.E. Shepherd. *Pulse detonation engine impulse analysis for partially-oxidized jet fuel.* Explosion Dynamics Laboratory Report FM2003.001, California Institute of Technology, April 2003.

[20] R. Akbar, P.A. Thibault, P.G. Harris, L.-S. Lussier, F. Zhang, S.B. Murray, and K. Gerrard. *Detonation properties of unsensitized and sensitized JP-10 and Jet-A fuels in air for pulse detonation engines.* (AIAA-2000-3592), 2000.

[21] A.A. Konnov. *Detailed reaction mechanism for small hydrocarbon combustion. Release 4.,* http://homepages.vub.ac.be/akonnov, 1998.

[22] N. Lamoureux and C.E. Paillard. *Natural gas ignition delay times behind reflected shock waves: Application to modelling and safety.* SHOCK WAVES, 13(1), 57-68, 2003.